Article

Evacuation of Shelter in Place at Subway Transfer Stations Based on BIM and Proposal of a Strengthening Method

Young-Hwi Kim [1], Jin-Seok Choi [2], Tian-Feng Yuan [2,*] and Young-Soo Yoon [2,*]

1   COO-WWS APAC Technical Sales Korea, Autodesk, Seoul 06164, Republic of Korea
2   School of Civil, Environmental and Architectural Engineering, Korea University, 125 Anam-ro, Seongbuk-gu, Seoul 02841, Republic of Korea
*   Correspondence: yuantianfeng@korea.ac.kr (T.-F.Y.); ysyoon@korea.ac.kr (Y.-S.Y.); Tel.: +82-2-3290-3320 (Y.-S.Y.)

Abstract: Among public facilities, facilities belonging to Multi-Group (I) include high-rise buildings, tunnels, and subway stations, and the location of Shelter in Place (SIP) is an important factor in the safety of citizens. However, subway evacuation maps usually induce evacuation to ground level or the tunnel of a subway platform without considering the location of SIP. In other words, since the location of the SIP is not determined, conditions, such as ventilation, air conditioning facilities, and structural durability required for the SIP cannot be satisfied. It is difficult to suggest the location of SIP because the domestic standards limit only the time it takes to move from the outside to the facility designated as SIP during an emergency evacuation. Therefore, in this study, when there is a situation of emergency evacuation in the subway, the total allowed time to evacuate to SIP is limited to 6 min. We designate a space that can accommodate the number of evacuees at the location and compare and analyze the results of the evacuation simulation using six scenarios. Additionally, suggestions are made for improvement methods relating to evacuation as well as the proposal of reinforcement methods through an experiment to satisfy the structural requirements of SIP in subway stations.

Keywords: building information modeling; evacuation simulation; shelter in place; impact resistance; shielding effectiveness

1. Introduction

Shelter in Place (SIP) is the act of seeking safety within the building one already occupies, rather than evacuating the area or seeking a community emergency shelter. The American Red Cross says a warning is issued when "chemical, biological, or radiological contaminants may be released accidentally or intentionally into the environment" and residents should "select a small, interior room, with no or few windows, taking refuge there" [1].

SIP has been included in earnest in building evacuation facilities since the enactment of the Basic Civil Defense in Korea [2]. Government-supported facilities refer to facilities installed within government subsidies in the five West Sea provinces (Baengnyeong, Daecheong, Socheong, Yeonpyeong-do, etc.) and military border areas. According to the Anti-Corruption and Civil Rights Commission [3], it can be defined by division into three categories as shown in Table 1. Designated facilities for public use include command and Chungmu facilities; Multi-Group (I) includes two stories below the basement of a high-rise building, subways, and tunnels; and Multi-Group (II) includes underground shopping malls, basements, walkways, and basements of multi-story buildings.

Other facilities may be the basement floors of small buildings, such as detached houses. A high-rise building included in Multi-Group (I) has a simple evacuation route because the evacuation space is in the basement or the evacuation floor using stairs or elevators. However, subway stations—especially those that are intricately entangled in the downtown

area—have complicated evacuation routes, and many stations overlap with one or more subway lines, requiring transfers.

Table 1. Designated facilities for public use (Seoul, Republic of Korea).

Categories	Target Facilities
Command and Control Center	Underground Facility Equipped with CBR (Chemical, Biological, and Radiological) Protection Facilities.
Multi-Group (I)	High-Rise Building (under the second basement floor), Subway, Tunnel, etc.
Multi-Group (II)	Underground Mall, Underpass, Underground Passage, Multi-Story Building (Basement), Civil Defense Training Center, and Underground Parking Lot.

As large-scale railway construction (Great Train Express (GTX)) has recently started, in the near future, major transfer stations will be linked with GTX, making the movement of users more complicated. Most subway stations in Korea have installed emergency evacuation maps detailing evacuation routes so that citizens using the subway are equipped with the means to respond quickly in the event of a situation for emergency evacuation. However, rather than designating the location of the SIP and providing an evacuation route, these guide movement in the direction of the tunnel away from the platform or outside of the subway.

According to "A Study on the Improvement of Civil Defense Resident Shelter Standards" [2], subway stations are national major facilities designated as Multi-Group (I) in Designated Facilities for Public Use in a CBRE situation. In the event of a CBRE situation, citizens must move to the SIP inside the station within 10 min [3]. However, these studies found no SIP-designated spaces or facilities inside the subway. In the case of subway transfer stations in Seoul, it is necessary to review the emergency evacuation escape time (6 min) suggested in "Design Guidelines for Convenience Facilities at Transit Stations" [4] because the underground space of the transfer station is larger than that of the general station, and thus the evacuation route may be longer.

This study simulates the case of evacuation by SIP and evacuation outside in the case of situations for emergency by targeting the subway transfer station with the most complicated evacuation route in the Multi-Group (I) category of Designated Facilities for Public Use. Regarding the location of the SIP, the optimal location in consideration of the evacuation route and acceptability with the complex station system will be studied.

In the case of structures designated as Designated Facilities for Public Use, structures that do not meet the structural standards of SIP or those that are over 20 years old should be excluded from SIP [2], and therefore the efficient structural reinforcement of old subway stations are also studied. Therefore, evacuation of SIP at Subway Transfer Stations based on BIM and the six types of strengthening method for the SIP structures are evaluated using static and low-velocity impact loading tests in this study.

2. SIP Simulation Based on the BIM Model

The subway station sampled in this study is Yangjae Station, where Subway Line 3 and Shinbundang Line meet. The study was conducted based on actual users of Yangjae Station on Line 3 and Shinbundang Line when calculating the variable work and evacuation number of the study. The necessary setting and assumptions are similar to previous research [4].

2.1. Variables for Evacuation Simulation

2.1.1. Movement of Occupants

Gait speed can be affected by personal physical conditions, such as height, weight, and leg length, as well as conditions, such as the evacuee's personality or surrounding conditions when a situation occurs [5,6]. According to a study conducted by Zou et. al. (2020) [7], the effects of human factors (i.e., emotion and perception) on crowd evacuation simulations

in emergency scenarios are emphasized. Usually V_e (m/s), the speed of pedestrians in an emergency scenario, is higher than V, the standard speed in the normal scenario [8]. Hence, the researchers confirmed that the walking speed differs according to normal and emergency conditions [7,8].

The purpose of the evacuation simulation of this study is that the location of the SIP is not actually defined at the subway station designated as a Designated Facilities for Public Use, and the evacuation route is guided to evacuate along the railroad tracks of the platform on which the train moves or to outside of the subway. This is to investigate whether evacuating to an outside location in the case of an emergency situation for the complicated routing of the transfer station is efficient regarding the evacuation time or if moving to the SIP is efficient if there is a space designated as SIP. Therefore, according to the above characteristics, the gait speed of pedestrians is classified according to physical requirements, such as age and gender, and the space where pedestrians are concentrated is affected by density [9].

Richard and Addison (2011) invetigated "Mitsugi Bone and Joint Study", "Hawaii Osteroporosis Study", "Study of Osteoporotic Fractures", "Halth Male; The average gait speed (horizontal) by gender and age in the United States, Sweden, the Netherlands, Australia, Japan, Canada, Israel, Germany, France, United Kingdom, Italy, and Kuwait was compiled based on ABS" and six other studies [10]. The horizontal gait speed was applied when creating the simulation profile in this study, and the gait speed under the age of 20 was determined through a study conducted by Ando et al. (1988) [11], as presented in Tables 2 and 3, which were applied based on the regression formulation.

Table 2. Regression formulation for the mean gait speed.

Gender	Age (Years)	Speed (m/s)
Female	2~8.3	$0.06 \times$ Age + 0.5
	8.3~13.3	$0.04 \times$ Age + 0.67
	13.3~22.25	$0.02 \times$ Age + 0.94
	22.25~37.5	$-0.018 \times$ Age + 1.78
	37.5~70	$-0.01 \times$ Age + 1.45
Male	2~5	$0.16 \times$ Age + 0.3
	5~12.5	$0.06 \times$ Age + 0.8
	12.5~18.8	$0.06 \times$ Age + 1.45
	18.8~39.2	$-0.01 \times$ Age + 1.78
	39.2~70	$-0.009 \times$ Age + 1.75

Table 3. Gait speed by age and gender.

Strata Gender (Age in Years)	Gait Speed (m/s)		Applied Speed
	Richard et al. [10]	Ando et al. [11]	
Men (0 to 9)	-	0.670 (0 to 1.340)	0.670
Men (10 to 19)	-	1.501 (1.400 to 1.602)	1.501
Men (20 to 29)	1.358 (1.270 to 1.447)	1.550 (1.490 to 1.610)	1.358
Men (30 to 39)	1.433 (1.316 to 1.550)	1.440 (1.480 to 1.399)	1.433
Men (40 to 49)	1.434 (1.353 to 1.514)	1.350 (1.309 to 1.390)	1.434
Men (50 to 59)	1.433 (1.379 to 1.488)	1.260 (1.219 to 1.300)	1.433
Men (60 to 69)	1.339 (1.266 to 1.412)	1.170 (1.129 to 1.210)	1.339
Men (70 to 79)	1.262 (1.210 to 1.322)	-	1.262
Men (80 to 99)	0.968 (0.834 to 1.101)	-	0.968
Women (0 to 9)	-	0.515	0.515
Women (10 to 19)	-	1.195	1.195
Women (20 to 29)	1.341 (1.239 to 1.443)	1.299	1.341
Women (30 to 39)	1.337 (1.193 to 1.482)	1.150	1.337
Women (40 to 49)	1.390 (1.339 to 1.411)	1.005	1.390

Table 3. *Cont.*

Strata Gender (Age in Years)	Gait Speed (m/s)		Applied Speed
	Richard et al. [10]	Ando et al. [11]	
Women (50 to 59)	1.313 (1.222 to 1.405)	0.905	1.313
Women (60 to 69)	1.241 (1.183 to 1.300)	0.805	1.241
Women (70 to 79)	1.132 (1.072 to 1.192)	-	1.132
Women (80 to 99)	0.943 (0.852 to 1.034)	-	0.943

2.1.2. Occupants Counting for Evacuation Simulation

Since the gait speed was defined by age and gender in 2.1.1, the evacuation population ratio was defined based on the results of the 2020 Population and Housing Survey of Statistics Korea in calculating the evacuation population (Table 4) [12].

Table 4. Population by age and gender (Units: thousands).

Ages (Years Old)	Population	Rate	Male Rate	Female Rate
0~9	3924	7.90%	4.20%	3.70%
10~19	4674	9.30%	5.00%	4.30%
20~29	6616	13.20%	7.30%	5.90%
30~39	6627	13.20%	7.00%	6.20%
40~49	7953	15.90%	8.20%	7.70%
50~59	8338	16.70%	8.40%	8.30%
60~69	6481	13.00%	6.20%	6.80%
70~79	3603	7.20%	2.50%	4.70%
Over 80	1917	3.80%	1.20%	2.40%
Total	50,133	100%	50.0%	50.0%

The number of evacuated people was calculated based on the actual user data of Yangjae Station (Seocho-gu Office), where Subway Line 3 and Shinbundang Line intersect. Seoul Transportation Corporation provides monthly subway user information through the corporation's website. In this study, Yangjae Station user information was used from December 2021. In the case of Yangjae Station, the busiest time of day was 8:00 am to 9:00 am, which is rush hour [13]. In the case of the Shinbundang Line, this is a subway that was constructed as a privately funded project and does not provide detailed user information in the same manner as the Seoul Transportation Corporation.

However, if the daily average number of passengers is compared with that of Line 3, and the number of passengers is inferred, the total number of those boarding and alighting at Yangjae Station on the Shinbundang Line in 2021 is 4,200,559, and the daily average number of boarding and alighting is 11,508 [14]. By inferring the number of passengers per hour on the Shinbundang Line based on the passengers at Yangjae Station, 263 passengers and 1442 alighters were calculated. Using the time when the largest number of passengers is concentrated in the subway station, the total number of people evacuated is 1007 based on 8:55, the overlapping time of the trains on Line 3 and the Shinbundang Line. Assuming three subway station staff members at each station and adding these to the evacuation number, the total number of evacuated people is 1013.

The number of people evacuated in the case of an emergency situation is the sum of the number of train occupants from the number of people waiting at the platform during peak hours. For the number of evacuees at the platform where the emergency situation has occurred, double the number of train occupants is considered as the simulation evacuation number, considering the number of passengers on the train that will be delayed by one train [4].

Therefore, the total number of evacuated persons is simulated by arranging the number of people who exited the train at Line 3 to 1454, which is twice the number of 727 people, assuming that the emergency situation occurred on Line 3, which has more passengers than

the Shinbundang Line. Therefore, the total number of evacuated people is 1454 deboarding and 132 people boarding line 3, and 126 people deboarding and 22 people deboarding at the Shinbundang line. In addition, the station staff was defined as three people each on Line 3 and Shinbundang Line, and the total number of evacuated people was calculated as 1740 people. Evacuees were automatically assigned according to the gender and age ratios defined in Table 4.

2.1.3. Location of SIP

It is explained that passengers should leave the platform within 4 min and exit a safe external entrance from smoke or toxic gas within 6 min [4]. Therefore, this study considers the case where all people in the station evacuate to the ground under the premise that the emergency situation has occurred and the case where they move to the SIP within the station. However, since the location of the SIP is not presented on the evacuation map as shown in Figures 1 and 2, the simulation was performed assuming the location of the SIP in a space that can accommodate the evacuation of people.
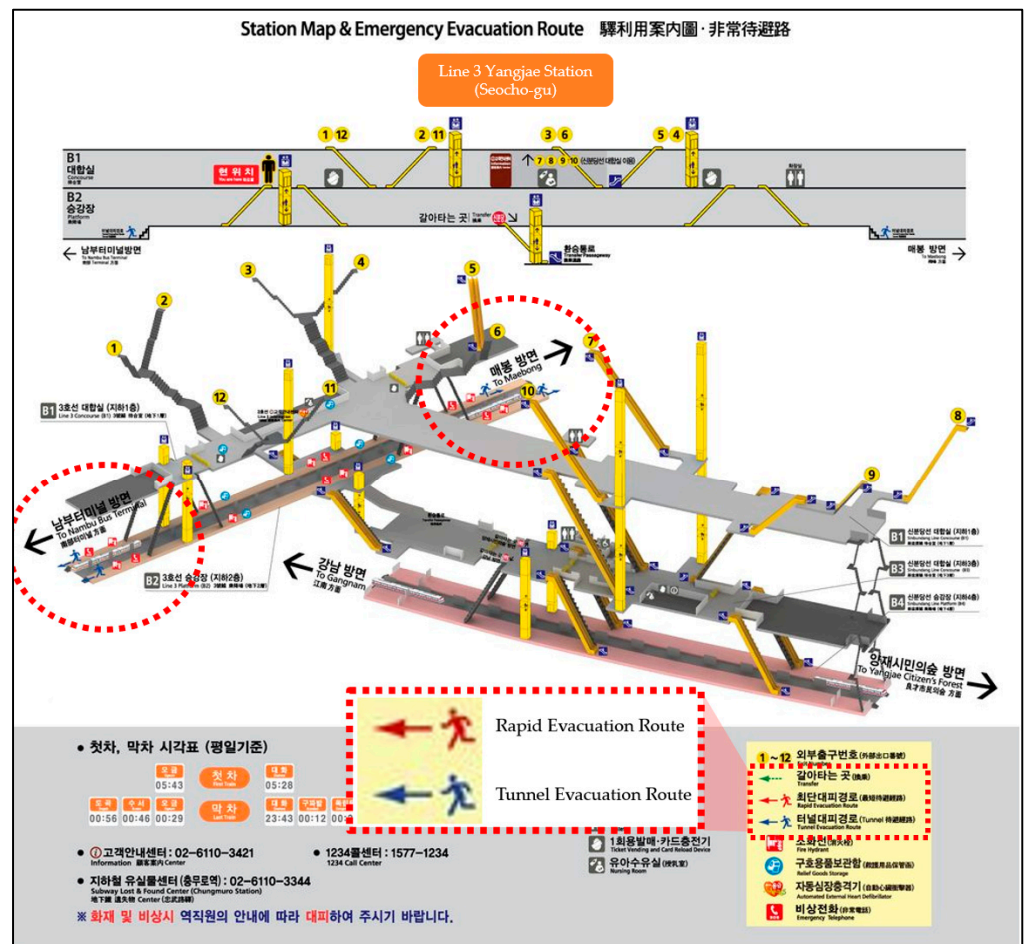

Figure 1. Station map and evacuation route.

As shown in Figure 3, Line 3 has a total of eight exits, and the Shinbundang Line has four exits. Although the recently completed Shinbundang Line has a large total area, the number of passengers on Line 3 is 12,453 in total and 1705 on the Shinbundang Line, which is 7.3-times more passengers than Line 3 based on the maximum usage hours. In order to determine the location of the SIP, it is necessary to consider the area of the space at each location.
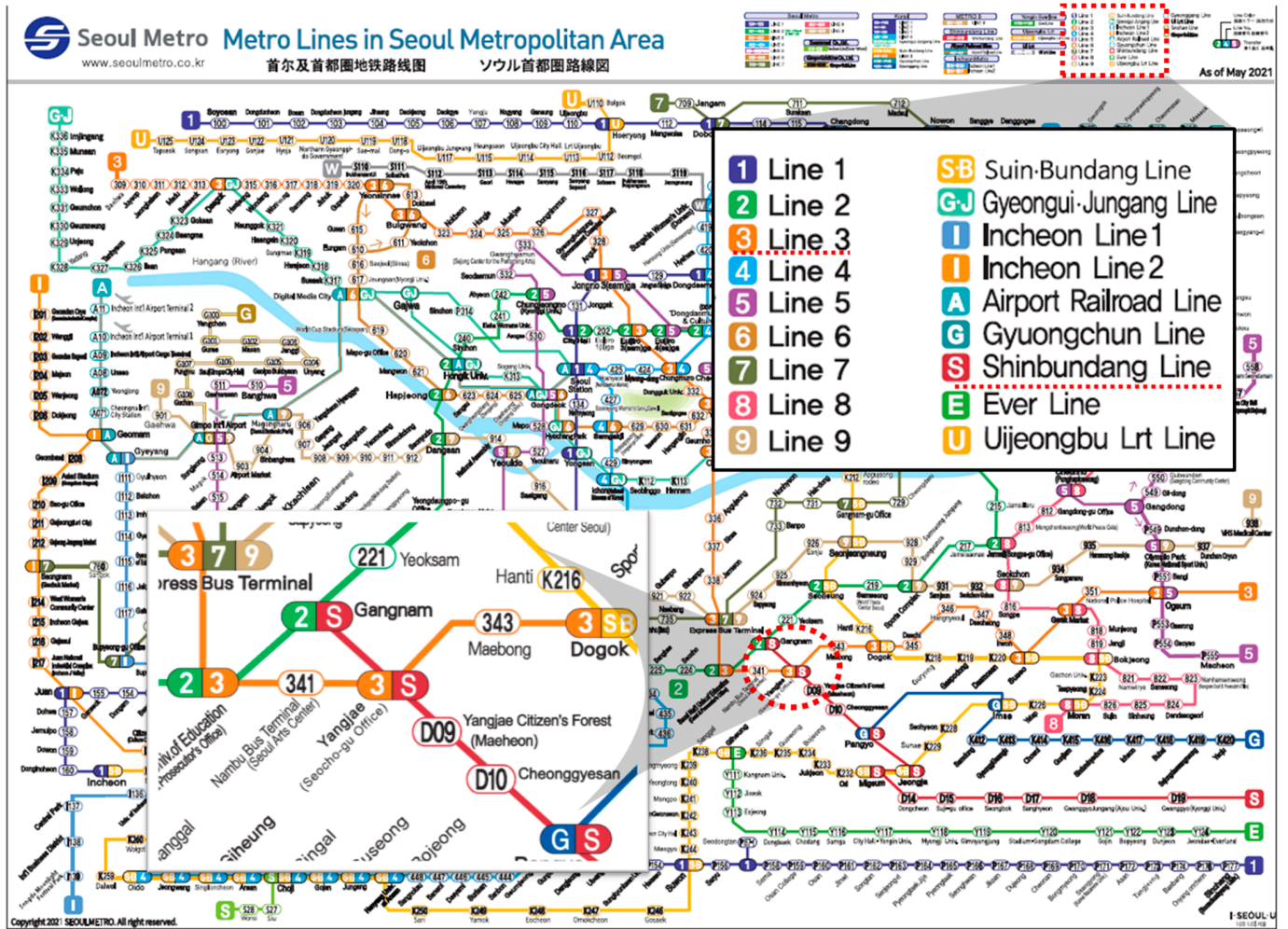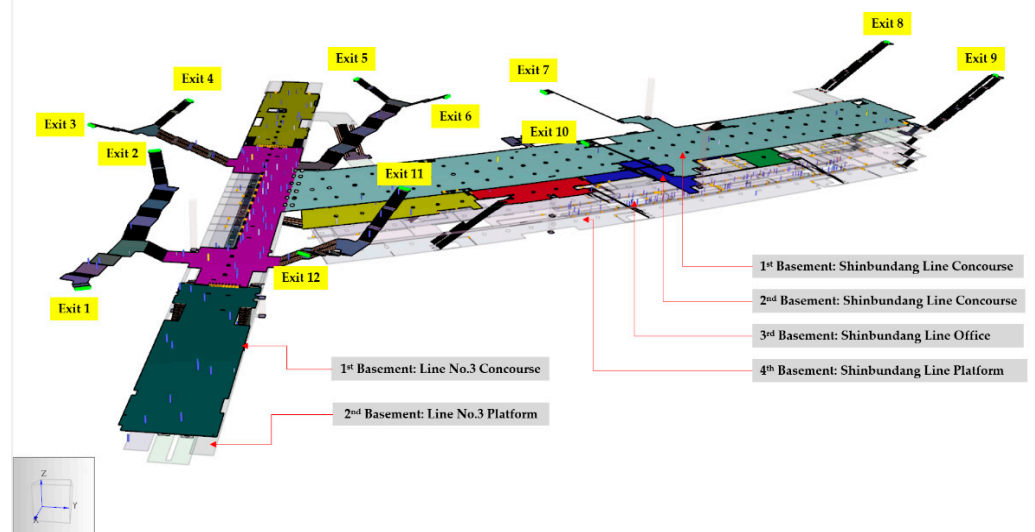
Figure 2. Seoul metro map.

Figure 3. Yangjae station layout.

In this study, the third section of the first basement floor of Line 3 and the first and second basement floors of the Shinbundang Line were considered as SIPs, and the location of the SIPs were adjusted according to the number of evacuees (Figure 3). The space required for sojourn is closely related to the stay time. In "A Study on the Improvement

of Civil Defense Resident Shelter Standards" [2], it was assumed that the period of stay is 2–3 days for Government-Supported Facilities and 10 h for Designated Facilities for Public Use.

FEMA453 (May 2006) defined as follows [15]:

a. Less Than 24 h. An occupancy duration of less than 24 h does not require sleeping areas. The occupant load will generally be a net 1.86 m^2/person, depending upon the classification of occupancy.

b. More Than 24 h. An occupancy duration greater than 24 h requires sleeping areas. The minimum floor area, with the use of single-size beds, is approximately 5.6 m^2/person. With the use of bunked beds, the minimum floor area is approximately 2.8 m^2/person.

In this study, Yangjae Station on Line 3 is composed of two floors as shown in Figure 4. The second basement platform has many exits, and thus it is helpful for evacuation. However, in the case of a train emergency situation, it is difficult to evacuate from the platform; therefore, it is difficult for the second basement floor to act as a SIP. Therefore, Area three on the second basement level of Line 3 was selected as a possible SIP location. Table 5 shows the capacity calculations of each SIP based on the area of each room designated as SIP and the number of people staying for less than 24 h as defined in FEMA453 [15].
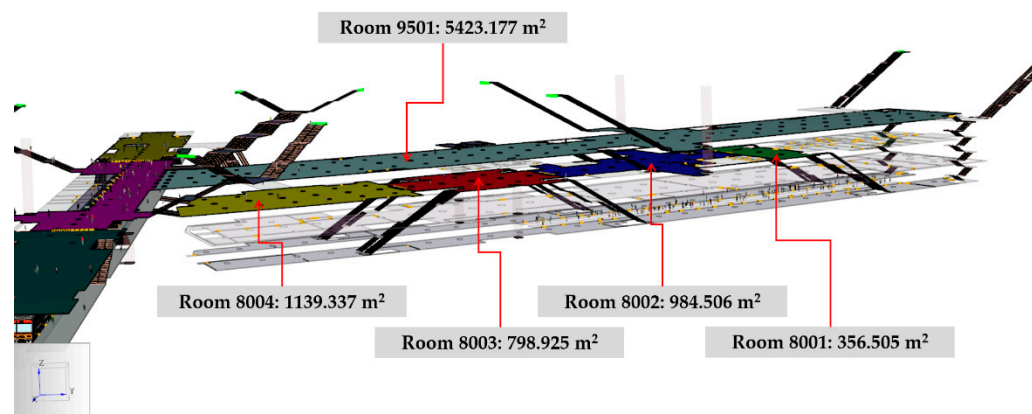

Figure 4. Line 3 SIP location and area.

Table 5. The Shelter in Place area and capacities (Yangjae Station).

Station	Room	Area (m^2)	Capacities (Persons)
	Room 7001	1077.908	580
Line 3	Room 7002	965.958	519
	Room 7003	1245.331	670
	Room 8001	356.505	192
	Room 8002	984.506	529
Shinbundang Line	Room 8003	798.925	430
	Room 8004	1139.337	613
	Room 9501	5423.177	2916

In the case of the Shinbundang Line and Line 3, the platform on the fourth basement level is unsuitable, and thus the first basement and second and third floors can be targeted. In the case of the third basement floor, access is poor as it is used and accessed only by internal facilities or station staff. Therefore, for the Shinbundang Line, the first and second basement floors with good accessibility were used as SIP targets and simulations were performed. The area and capacity of each site are shown in Figure 5 and Table 5.

Figure 5. Shinbundang line SIP location and area.

2.2. Modeling

In this study, Yangjae Station modeling was performed using Autodesk Revit and AutoCAD, which are mostly used for BIM modeling. Evacuation simulation was performed using Thunderhead Engineering's Pathfinder. This was adopted as it satisfies all standards of the IMO (International Maritime Organization) guidelines that are currently used for the verification of evacuation programs [16,17].

2.2.1. Creation of a Mesh

Pathfinder utilizes many parameters in its modeling using shape information to define components, such as room, stair, door, escalator, and many more in the form of a mesh. For example, in the case of a room composed of multiple meshes, each node of the mesh created for simulation must be shared with the others. Errors or path detours will result in incorrect simulation results. Therefore, since the mesh is the most basic shape information of the elements used in the evacuation simulation, it can be said that the management of the mesh is important in the simulation.

2.2.2. Door

Generally, in the case of a door, this is a point within the simulation or event where occupants are bottlenecked during the evacuation process and is, therefore, an important structure that greatly impacts the evacuation time. However, the evacuation route of Yangjae Transfer Station sampled in this study moves from the platform on the second basement level of Line 3 and the fourth basement floor of the Shinbundang Line to the first basement level using stairs or escalators and then moves to the ground level. Therefore, the spaces mainly by occupants are the first and second basement floors of Line 3 and the Shinbundang Line (Figure 3). There are few doors that must be passed through on the evacuation route.

However, when moving from the subway to the platform, it is necessary to pass through the subway doors and screen doors, which can become a bottleneck during times when there are many subway users. Trains operating on Subway Line 3 are: Seoul Metro 3000 series Chopper-controlled EMU, Seoul Metro 3000 series Chopper-controlled EMU (rebuilt cars), Seoul Metro 3000 series VVVF inverter-controlled (first generation), Korail Class 3000 (first generation) [18], all of which consist of 10 cars. The trains on the Shinbundang Line are DX line series D000 cars and operate based on six cars, which is four cars smaller than Line 3 [18]. Therefore, in the simulation, if the width, length, and the number of trains are equally considered in relation to the bottleneck when exiting the train, the width of the train is set to 1.3 m [19].

2.2.3. Gate

The ticket gates of the subway are largely divided into three-leg and sensor types, and all ticket gates at Yangjae Station use the sensor type. In consideration of the disabled, at least one of the counting stations was installed with a width of 800 mm or more [20], and the standard width of the general counting gate was not provided; thus, 600 mm was used, which was confirmed by actual measurement. In addition, a delay time of 1 s was applied when passing through the gate due to the process of taking, recognizing, and accepting a transportation card.

The ticketing gate only allows passing in one direction; however, the simulation shows that the number of people deboarding at the morning rush hour is greater than the number of people on board. Therefore, the number of gate passages was increased from the platform to outside. The gates located in the direction of exits 1, 2, 11, and 12 of Yangjae Station consist of nine passages, eight passages for the general public, and one passage for the disabled. Four were assigned in each direction, and by setting the disabled people to move outside, the settings were defined more advantageously for moving outside (Figure 6). This was defined in consideration of the fact that the number of people exiting at work hours is high, and we confirmed that the actual station is operated in the same way.
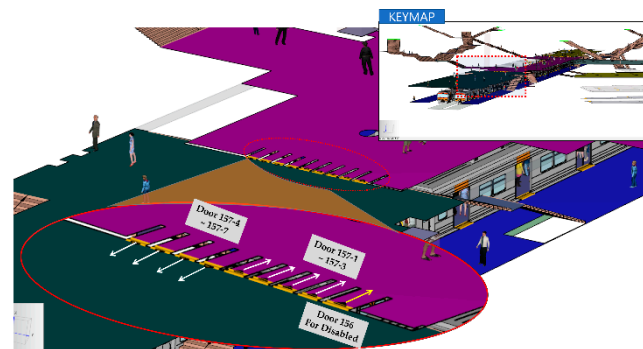

Figure 6. The gate arrangement of line 3.

2.2.4. Elevator and Stairs

The major difference between an escalator and a staircase is that a staircase is static and can move in both directions, whereas an escalator only moves in one direction at a constant speed. The shape of the stairs affects the pedestrian speed. A lower riser and higher tread leads to a positive effect in the evacuation speed [5,6]. After modeling the escalator with a ramp, it was defined to move in one direction by designating the upward and downward directions. The Line 3 station does not have an escalator and is installed only on the side of the Shinbundang Line. The speed of the escalator is suggested to be 0.5 m/s to 0.67 m/s in the elevator convenience facility installation standard of the Main Design Criteria for Subway (Facility Field). In this study, this was conservatively defined as 0.5 m/s [21,22].

2.2.5. Occupant

In this study, as shown in Table 3, gait speed was defined by age and gender. Therefore, all evacuation people were classified as pedestrians according to the ratio defined in Table 4. The estimated 1740 people evacuated was based on 8:55 am when the subway train had arrived, and we assumed that all alighted people were on the train. Rather than deboarding the train and moving, this was judged to be disadvantageous during the evacuation time because they had to go through a narrow door to exit the train. Therefore, we assumed that 1454 people were on Line 3 and 126 people were on the Shinbundang Line, and the number of passengers was evenly arranged on the first and second basement floors of Line 3 and the first, second, and fourth basement floors of the Shinbundang Line (Figures 6 and 7). In this study, the simulation assumed the busiest time to go to work; therefore, people with disabilities were not considered.
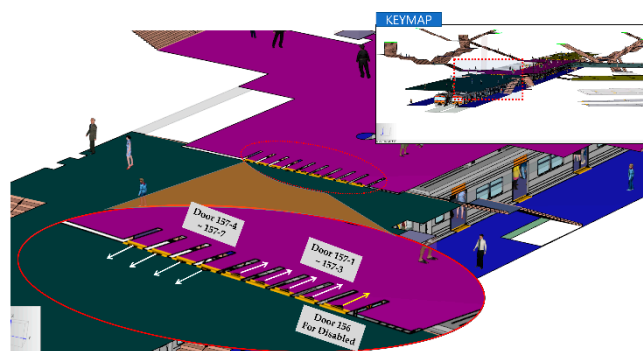
Figure 7. The Line 3 occupant arrangement layout.

2.3. Scenario

In the event of the emergency situation in the subway, the evacuation time standard defines that all passengers must leave the platform within 4 min and exit a safe external entrance from smoke or toxic gases within 6 min [4]. However, out of 291 subway stations in Seoul, 90 stations (31%) are stations where two lines are merged, and 12 stations (4%) are stations where three lines transfer. Considering the GTX and the new lines in the future, Gimpo Airport Station or Seoul Station will become stations where up to five lines transfer from the existing two lines to the Gimpo Urban Railway and the Seohae Line. As such, in the case of a transfer station, the movement line to the outside is longer than a station where only one line stops, and depending on the movement line, there is a high possibility of overlapping or bottlenecks of pedestrians.

If you check the Station Map and Emergency Evacuation Route of subway stations in Seoul, the location of the SIP is not determined, and most of the evacuation routes are guided by moving to the outside or evacuating from the platform to both tunnels. (Figure 1) A subway station is a national major facility designated as Multi-Group (I) in the Designated Facilities for Public Use in a CBRE situation. However, as shown in Figure 1, if it moves to the outside or the tunnel next to the platform, it cannot be considered as a proper SIP.

Therefore, this study examines whether the evacuation time is satisfied for a long evacuation route in the case of the emergency situation by targeting Yangjae Station, which is actually a transfer station, and studies where the most optimal location is when there is an evacuation space. As a result, scenarios were simulated where all evacuees went outside, moved to the first or second basement floor of the Shinbundang Line, and moved to the first basement floor of Line 3 and the second basement floor of the Shinbundang Line, respectively (Figures 4 and 5).

In general, a bottleneck occurs at the door or stairs leading to the emergency stairs in a subway station; however, when many people are deployed in a large space, such as a transfer station, the bottleneck occurs at the subway gate. In the case of Yangjae Station, unlike other stations, the larger open space and wider access ways greatly reduce the presence of bottlenecks; however, bottlenecks still occur at the gate as it is necessary for people to pass through. The gate does not move in both directions and only moves in one direction; this can have a great impact on the evacuation time. Therefore, additional simulations are conducted by adjusting the gate conditions in the five scenarios in Table 6.

Table 6. Scenario description and SIP location.

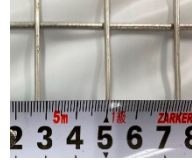| Scenario	Description	SIP Location
Scenario A	Evacuate at the exit of Line 3 and Shinbundang Line	Exits: 1~12
Scenario B	Evacuate to the second basement floor of the Shinbundang Line	Rooms: 8001~8004
Scenario C	Evacuate to the first basement floor of the Shinbundang Line	Rooms: 9501
Scenario D	Evacuate to both sides of the first basement floor of Line 3 and the second basement floor of the Shinbundang Line	Rooms: 7001, 7002, 8001, 8002, 8003, and 8004
Scenario E	Evacuate from the center of the first basement floor of Line 3 and the second basement floor of the Shinbundang Line	Rooms: 7003, 8001, 8002, 8003, and 8004

3. Strengthened Method for SIP

In general, the outer wall in contact with the soil is 300–500 mm, which meets the structural condition requirements; however, the inner wall is 100–200 mm, which does not satisfy the wall conditions for SIP [2]. Therefore, the method of strengthening the existing walls and beams to perform the structural role of SIP is studied. The strengthening methods were directed mainly for impact resistance and electromagnetic interference shielding (EMI) effectiveness in this study.

3.1. Details of Test Specimens

This study used high-strength high-ductility concrete (HSDC) to strengthen the normal-strength concrete (NSC) beam and wall elements to improve the impact resistance. According to previews research, the strengthening material HSDC has great mechanical properties (strength and energy absorption) [23,24] and bond strength [25]. NSC beams strengthened with a different method by HSDC showed an improved yield and ultimate capacity based on the static load testing [25]. Additionally, the NSC wall strengthened by metallic mesh [Table 7] was evaluated in order to analyze the EMI shielding effectiveness. These test data were helpful not only during the design of the strengthening method of beams and/or walls but also support a clear idea of the likely resistance improvement of the structural elements under impact and/or shielding effectiveness. All the test specimens were tested after curing for 28 days in this study.

Table 7. Properties of the metallic meshes.

	M5	M10	M25
Types			
Diameter (mm)	0.73	1.18	1.90
Tensile strength (MPa)	987/1013	836/821	842/866

3.1.1. Materials

The reinforced concrete elements were fabricated from normal-strength concrete (NSC), which consists of water, type I Portland cement (ATSM C150 [26]), crushed fine aggregate, and coarse aggregate with a maximum size of 18 mm. The compressive and flexural strengths were 44.6 and 25.7 MPa at 28 days, respectively. The strengthening material HSDC consists of water, type I Portland cement, silica fume with a density of 2.20 g/cm^3 and a specific surface area of 200,000 cm^2/g, filler with a density of 0.75 g/cm^3 and a specific surface area of 2.65 cm^2/g, silica sand with the diameter ranging from 0.08 to 0.30 mm, and hybrid 1.0 vol.% high-strength straight steel fiber and 0.5 vol.% of high-strength polyethylene fiber as shown in Table 8. The compressive strength, flexural strength,

direct tensile strength, and tensile strain occurred at 122.3 MPa, 22.9 MPa, 9.7 MPa, and 2.97 mm/mm, respectively.

Table 8. Mixture proportions (by weight).

Types	*w/b*	Water	Cement	Silica Fume	Silica Filler	Sand	Coarse Aggregate	Steel Fiber	Polyethylene Fiber	SP
NSC	0.43	0.43	1.00	-	-	2.15	2.42	-	-	0.8%
HSDC	0.172	0.215	1.00	0.25	0.30	1.10	-	1.0%	0.5%	3.0%

NSC = normal-strength concrete; HSDC = high-strength high-ductility concrete; *w/b* = water-to-binder ratio; Sand: NSC uses crushed fine aggregate, and HSDC uses silica sand; and SP = superplasticizer.

3.1.2. Specimen Details

The reinforced concrete beams were designed to be 125 mm in width, 250 mm in height, and 2222 mm in length. The flexural reinforcement requirements were met with two D19 bars, and U-shaped opened 8 mm round and smooth steel bars were used to resist the minimum shear strength capacity (NC-NN). According to a previous study [25], NSC beams strengthened by HSDC on the bottom side or on both the top and bottom sides were not meaningful to improve the structure properties without shear reinforcement rebar. NSC beams using jacketing on three sides and jacketing on four sides can significantly improve the structural properties and exhibited flexural failure modes without shear reinforcement.

Therefore, two types of strengthening methods consisting of NSC beam specimens without (NC-NN) shear reinforcement were used, which was chiseled to a 40 mm depth on the bottom side and 20 mm on the top as well as on the two vertical sides. Therefore, the jacketing on the bottom and two vertical sides (NC-3J) and jacketing on the four sides (NC-4J) based on NC-NN were prepared as shown in Figure 8a. For the reinforced concrete walls, two specimens related to size were implemented. First, the 300 × 300 × 100 mm specimen was used to evaluate impact the resistance and shielding effectiveness.

(**a**)

(**b**)
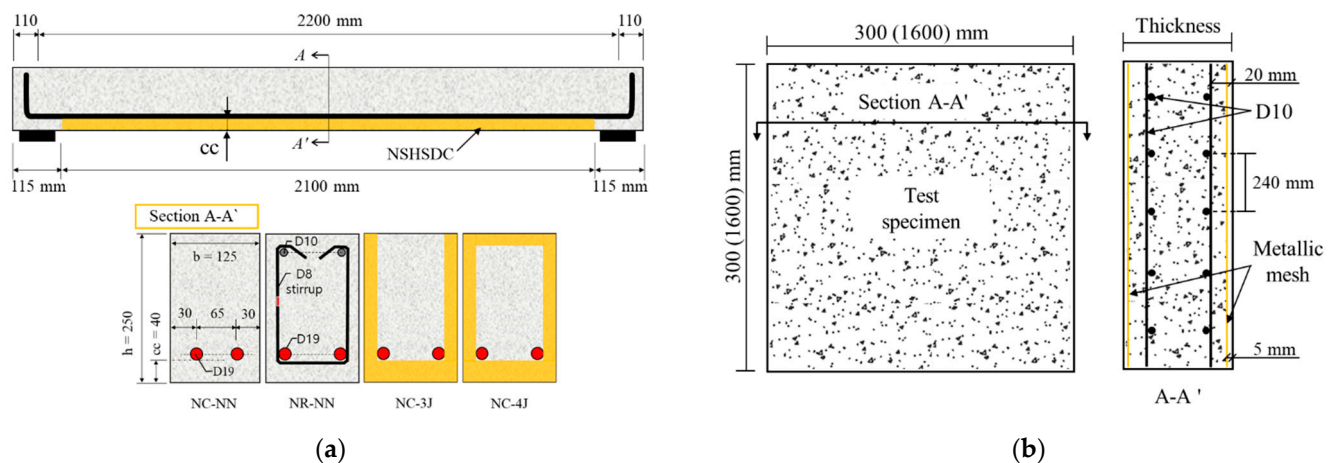
Figure 8. Strengthening details of test specimens. (**a**) Details of the test beams. (**b**) Details of the test walls.

In addition to these tests, the 1600 × 1600 × 1400 mm specimen also saw screening strengthening tests. Therefore, small size specimens were used to consider the strengthening capacity without steel bar reinforcement, and large-size specimens were reinforced using double-layer D10 steel rebar in both directions. The details are shown in Figure 8b and Table 9, and all the specimens were cured in a room at a temperature of 20 ± 1 °C and humidity of 60 ± 5% until the test day.

Table 9. Properties of the metallic meshes.

			Specimens Thickness (mm)	Strengthening Materials					
				Metallic Mesh			HSDC		
				5 mm	10 mm	25 mm	5 mm	10 mm	20 mm
1		S-NC		-	-	-	-	-	-
2	Type I	S-M5		double	-	-	-	-	-
3		S-M10		-	double	-	-	-	-
4		S-M25	100	-	-	double	-	-	-
5		S-H5		-	-	-	double	-	-
6	Type II	S-H10		-	-	-	-	double	-
7		S-H20 D		-	-	-	-	-	double
8		L-NC		-	-	-	-	-	-
9	Type III	L-M5	140	double	-	-	-	-	-
10		L-H20		-	-	-	-	-	double

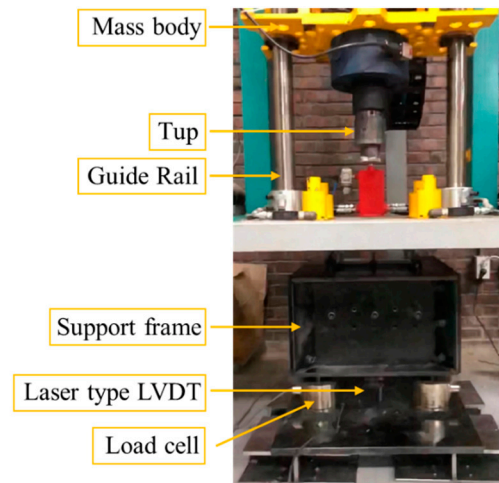*3.2. Test Setup*

3.2.1. Impact Test

The impact drop-weight test equipment for beams and large-sized wall specimens is constitutive of the hydraulic release system, mass body (300 kg), guide rail (steel H-beam with 150 × 150 × 75 mm), and supports as shown in Figure 9. The load cells (a maximum capacity of 490 kN) were installed at the each support (two and four load cells used in the beam and slab tests, respectively) to measure the reaction force. All beam and wall specimens were tested under the free fall of a 300 kg hemispherically shaped tup (150 mm in diameter) at 2000 mm, which imparted impact energy of approximately 5.9 kJ at a velocity of 6.3 m/s.
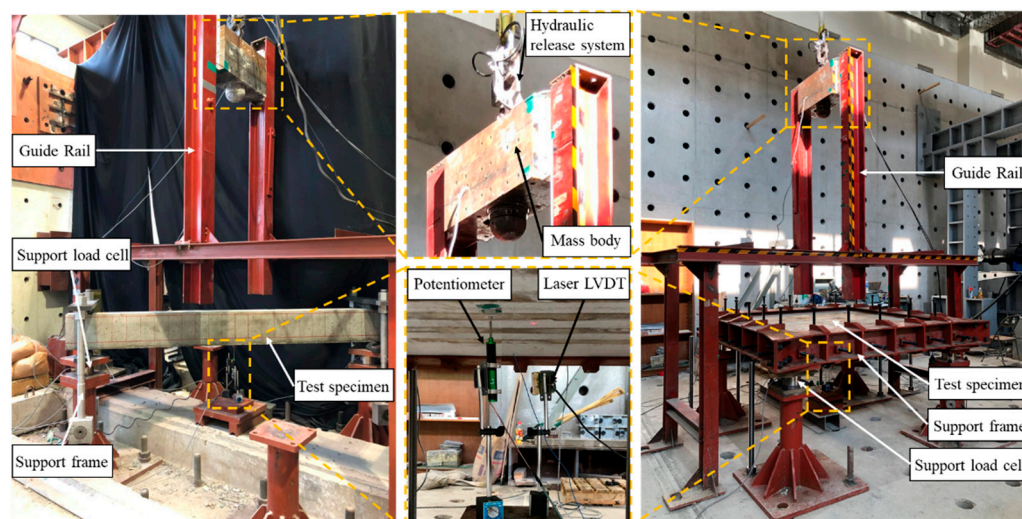
Figure 9. Test setup of drop-weight impact test for beam and large-sized wall specimens.

In order to measuring the maximum and residual displacement at the mid-span of the test beam, the potentiometer (100 mm, JCL 100B) and laser LVDT (120 mm, KL4-120NV) were placed on the bottom surface of the test beam. The load cells, potentiometer, and laser LVDT were connected to a dynamic data logger (DEWE-43, Trbovlje, Slovenia) for data acquisition. The sampling rate was adopted as 100 kHz in order to acquire adequate data based on previous studies, which is important for measuring reliable data from drop-weight impact testing [27,28].

For small-sized wall specimens of the impact drop-weight test equipment, we adopted a user-defined setup specifically made for such evaluations as shown in Figure 10. The conception refers to large-size impact test equipment, and the compressed specimen uses

C-shaped steel supports around four sides to prevent rebounding upon impact. A 100 kg mass free-fall test method was adopted for small-sized specimens, with the initial drop location at a height of 200 mm and increasing by 100 mm at each increment.

Figure 10. Test setup of the drop-weight impact test for beam and large-sized wall specimens.

3.2.2. EMI Shielding Test

The EMI shielding effectiveness test equipment utilized the near-field condition test method equipment with a frequency range of 300 to 1500 MHz on the use of the transmitting and receiving facility [29–31] as shown in Figure 11. Before measuring the shielding effectiveness of the specimen(s), calibration was applied for every measurement to ensure correct evaluation of the nominal value on the receiver. The distance between the transmitting and receiving log-spiral antennas to the test wall was calibrated to be 20 mm. The EMI shielding test was repeated five times for each test wall, removing the maximum and minimum values and utilizing only the average values of each specimen in this study.
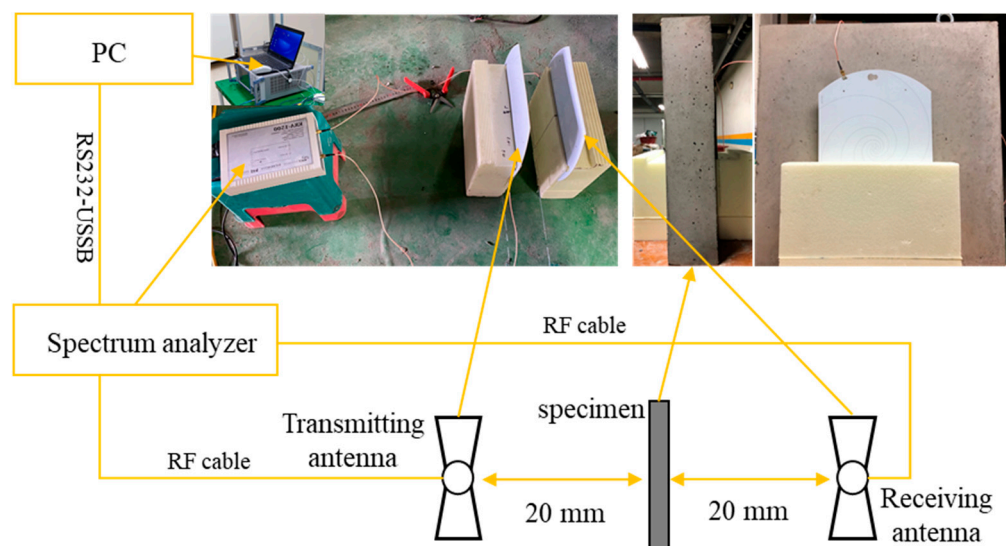
Figure 11. Test setup of the EMI shielding test.

4. Results and Discussion

4.1. Scenario Based on the Location of the SIP

4.1.1. Scenario A

In the case of Scenario A, a total of 1740 people in an emergency situation are evacuated through 12 exits. Among the total number of evacuees, the number of evacuated passengers

on the Shinbundang Line was 126 people on board, 22 people deboarding, and three subway station crew, for a total of 151 people. Therefore, most of the people evacuated are concentrated in Line 3. There are eight evacuation exits on Line 3 (Figure 3), and 1589 people are evacuated through eight exits. A bottleneck occurs in front of the gate (Figure 8). The reason the maximum flow rate does not exceed 0.5 persons/s is that, as mentioned in Section 2.2.3, the time (1 s) that the gate sensor recognizes after touching the transportation card when passing through the gate is assumed in the simulation to be from 47.98 to 475 s.

The bottleneck at the gate is a factor that greatly affects the total evacuation time. In the case of Scenario A, the total evacuation time is 529.6 s, and the maximum travel distance is 324 m. This is 169.6 s (2.82 min) longer than the 6 min required to evacuate from smoke or toxic gas in the case of an emergency situation mentioned in the "Guidelines for Design Guidelines for Convenience Facilities at Transit Stations for Urban Railroad Stations" [4]. Therefore, we confirmed that the method of evacuation by exiting to the surface is not sufficient at subway stations with long and complex structures, such as transfer stations.

4.1.2. Scenario B

According to the results of Scenario A to evacuate outside in the case of an emergency situation, the evacuation time was delayed by 169.6 s (2.82 min) and was unable to evacuate within the 6 min of allowable evacuation time. Currently, most subway facilities are designated as SIP; however, no SIP space is designated within the facility. Therefore, from Scenarios B to E, assuming the location of the SIP space, we conducted a simulation and determined whether the allowable evacuation time was satisfied. First, in Scenario B, the second basement floor of the Shinbundang Line was designated as the SIP space. All four spaces (Figure 5) from Room 8001 to 8004 were designated as SIPs, and simulations were performed.

In the case of the B2F of the Shinbundang Line, it consists of four rooms, where the space available for SIP is 3279.573 m^2 in total, which can accommodate 1763 people (Table 5). There are two evacuation routes: the passage from the platform on the second basement level of Line 3 to the second basement level of the Shinbundang Line, and the passage from the first basement floor to the Shinbundang Line. In Figure 9 Section A, as evacuees flocked to the gate, a serious bottleneck occurred as the people who exited the train at Subway Line 3 in the Maebong and Nambu Bus Terminal directions (Figure 1) moved to the passageway connecting the B1 and B2 floors of the Shinbundang Line.

In the case of Section B in the opposite direction, there was a connection passage that went directly to the Shinbundang Line without passing through the gate after moving to the first basement floor, and thus there was no congestion at the gate. We also confirmed that the bottleneck occurred at the transfer gate as the evacuees who first moved to Room 8004 moved to Room 8003 located inside.

The evacuation of evacuees was defined so that they could move in a proportionate way considering the capacity of each room. Finally, Room 8001 accommodates 191 people, Room 8002 accommodates 529 people, Room 8003 accommodates 430 people, and Room 8004 accommodates 590 people for a total of 1740 people. The maximum evacuation time was 427.6 s, and the maximum travel distance was analyzed to be 287.6 m. All of these were 102 s and 37.2 m shorter than Scenario A; however, evacuation within 360 s (6 min) still failed. When the capacity of each evacuation space was specified, evacuees were stuck in the room.

In order for evacuees to move to the SIP, they must pass through the gate; however, if the time delay at the gate exceeds the capacity of the room, evacuees cannot pass through the room and are trapped in the room. Therefore, in Scenario B, even if the capacity of the room is limited, there is adequate space allowing for SIP utilization. Hence, when evacuating, it is defined so that only the evacuees can be assigned to accurately determine their room while ignoring the accommodation space of the room. The room to which specific evacuees move was not defined separately but the ratio was defined for each group

of evacuees. Evacuees on the New Bundang Line were defined to move to the nearest Room 8001 because there were not many people, and the number of people who left the train at Line 3 was defined in proportion to the capacity of Rooms 8002, 8003, and 8004.

4.1.3. Scenario C

In Scenario C, an evacuation simulation was performed under the same conditions as Scenario B, assuming that the SIP space is the first basement floor of the Shinbundang Line. Room 9501 on the first basement floor of the Shinbundang Line has an area of 5423 m^2 and can accommodate 2916 people, making it a suitable space. However, as a result of the simulation, a serious bottleneck occurred in section A and section B, both gates of Line 3, delaying the evacuation time (Figure 10). As a result, in the case of Scenario C, the maximum evacuation time was 457.8 s, which is 71.8 s shorter than that of Scenario A, and the maximum travel distance was 288.2 m, which is 36.6 m shorter than that of Scenario A.

In Scenario B, it was expected that the evacuation time would take longer than in Scenario C because there is a gate when moving to each room. However, as in Section A of Figure 10, we confirmed that the evacuation time was shortened compared to Scenario C because it moved to the second basement level of the Shinbundang Line without passing through the gate. In conclusion, we confirmed that the case of using the first basement floor of the Shinbundang Line as an evacuation site was disadvantageous in terms of the evacuation speed compared to the second basement floor.

4.1.4. Scenario D

In the case of Scenario D, the location of the SIP was defined as the second basement floor of the Shinbundang Line (Room 8003 and 8004) and the inside of the gate on the first floor of the Line 3 (Room 7001 and 7002). Evacuees on the Shinbundang Line evacuate to the nearest shelter, Room 8003, and evacuees on Line 3 consider the movement of evacuees in the Maebong direction and evacuate to the shelters on both sides of Line 3, 7001 and 7002. Evacuees in the direction of Nambu Terminal were set to evacuate to Room 8003 and 8004 on the second basement floor of the Shinbundang Line, which are close to each other.

This is to simulate the evacuation by moving the evacuation route as close as possible to scenarios A, B, and C, because the evacuation route was long or the bottleneck occurred at the gate, and thus the evacuation could not be done within the allowable evacuation time. As a result of the simulation, the maximum evacuation time was 236.1 s, which was 293.5 s shorter than the maximum evacuation time of Scenario A, and the evacuation distance was also shortened by 93.1 m from 324.8 m in Scenario A to 231.7 m. This is because the evacuation site was set in a place that does not pass through the gate in order to reduce the evacuation time by minimizing the evacuation route that greatly affected the evacuation time as well as to reduce the bottleneck that occurs at the gate.

4.1.5. Scenario E

In this study, simulations were performed assuming the situation when an emergency situation occurs in the subway station or subway Line 3. If the emergency situation breaks out between the platform on the second basement floor of Line 3 and the passageway on the second basement floor of the Shinbundang Line, it may be impossible to move there if the fire shutter comes down. In this case, since they have to travel to the first basement floor and move in the direction of the Shinbundang Line, the remaining people, except for the number of people who can be accommodated in Room 7001 and 7002, are moved to Room 8003 and 8004 of the Shinbundang Line to perform the simulation.

As a result of the simulation, the people from the second basement floor of Line 3 moved to the first floor, creating a bottleneck in front of the Section B gate, which was expected to cause congestion. However, after the evacuees moved from the second basement to Section A of the first basement floor, the simulation proceeded without any particular congestion as they moved to the Shinbundang Line without passing through the gate (Figure 11). Due to the longer evacuation route, the maximum evacuation distance

was 277.3 m, 45.6 m longer than in Scenario D, and the evacuation time was delayed by 116.7 s, resulting in a maximum evacuation time of 352.8 s. This satisfies the allowable evacuation time of 360 s, resulting in the most efficient evacuation space on both Line 3 and Shinbundang Lines.

4.1.6. Scenario F

Scenarios D and E defined Room 7001 and 7002 of Line 3 as SIP; however, in Scenario F, SIP was defined as Central Room 7003. However, while Room 7001 and 7002 have an area of 2044 m^2 and can accommodate 1099 people, Room 7003 is 1245 m^2 and can accommodate 670 people. For the remaining 429 people, an evacuation simulation was performed by adding Room 8002, which can accommodate an additional 529 people, in addition to Room 8003 and 8004 in the evacuation spaces of the Shinbundang Line. In Scenario F, there was congestion at the gate as evacuees moving from Section B to Room 7003 and the Shinbundang Line flocked.

We confirmed that the evacuation was smoother than Section B because the route to the evacuation was possible without passing through the gate. We also confirmed that a bottleneck occurred at the transfer gate as evacuees moved from Room 8004 to Room 8003 flocked (Figure 12). Simulation results showed that the maximum evacuation time was 474.6 s, which is 238.5 s longer than in Scenario D. As the evacuation space was moved from the existing Room 7001 and 7002 to the narrow Room 7003, and 8002 on the Shinbundang Line was added as an evacuation space to accommodate the rest of the evacuees, increasing the evacuation distance. The maximum evacuation distance was 305.2 m, which increased by 73.5 m compared to Scenario B.
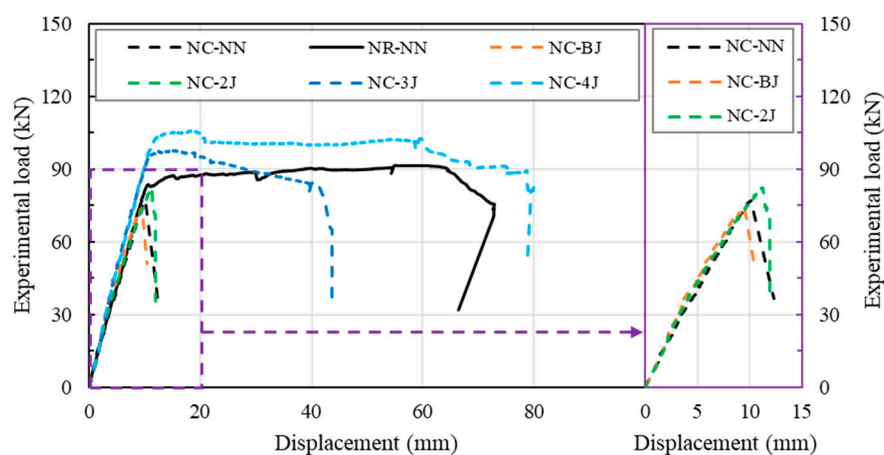
Figure 12. The load-deflection behavior of the test beams.

4.2. Improvement Method for Evacuation

As reviewed in Section 4.1, subway stations are designated as Designated Facilities for Public Use Multi-Group (I) and are safe places for civilians to evacuate in CBRE situations. Additionally, it is more efficient evacuating to an SIP located in an advantageous location within the subway, rather than evacuation through the external entrance in the case of the emergency situation due to the complications and length of moving paths in situations, such as transfer stations.

A comprehensive review of the preceding Scenarios A to F shows that most of the evacuation time was spent at the subway gate. In the case of a tripod gate, it may be difficult to perform an evacuation simulation after changing the following conditions; however, in the case of Yangjae Station sampled in this study, sensor-type gates are used. Therefore, for all the scenarios reviewed in Section 4.1, simulations were performed by changing only two conditions related to the gate below under the same conditions.

First, we set the directions of the gate to both directions so that evacuees moved in both directions. Second, when passing through the gate, all delay time was removed by

ignoring the delay time due to traffic card tagging and assuming that it is possible to pass through.

The results of review after setting the above two items were as follows (Table 7). As a result of the simulation, we analyzed that all evacuees were able to evacuate within 6 min, which is the allowable evacuation time, except for scenarios B and F. In Scenarios A and C, the times were shortened by 271.7 and 251.7 s, respectively, and the maximum evacuation distances were also greatly shortened to 85.8 and 107.8 m, as both scenarios had more people passing through the gate than the other scenarios.

4.3. Performance of Test Beams with Different Strengthening Methods

4.3.1. Static Loading Resistance Capacity of Beams

Figure 12 shows the load relative to the mid-span deflection curves obtained from static flexural tests. Yuan et al. (2020) [25] presented that normal-strength concrete beams without shear reinforcement (NC-NN) strengthened with HSDC on the bottom side and top/bottom side (NC-BJ and NC-2J) exhibited shear failure without any increases in the mechanical properties. However, the NC-NN specimens strengthened with three and four sides (NC-3J and NC-4J) exhibited 6.7% and 15.9% higher ultimate loads compared to NC-NN with a shear reinforcement beam (NR-NN, 91.58 kN).

The inhomogeneous steel and polyethylene fiber distribution and orientation of HSDC affected the flexural performance of the test beams. It should be noted that increasing the number of strengthening sides leads to the specimen becoming over-reinforced, causing the strengthening beams to experience a considerable loss of ductility [25,32–34]. Hence, as the HSDC with a large number of strengthening sides, distribution, and propagation of cracks, the test beam NC-4J exhibited not only an improvement in the ultimate strength but also an increase in the energy absorption, which was approximately 24.1% (7.11 kN·m) higher than specimen NR-NN (5.73 kN·m).

The combined contribution of four sides strengthened by HSDC improved the structure properties (peak load, deflection, and crack distribution), compared to other test specimens. For all normal-strength concrete beams strengthened with HSDC, bond failure did not occur in the static loading test, which detailed the great bond-strength properties between HSDC and NSC [25].

4.3.2. Drop-Weight Impact Resistance Capacity of Beams

The variation of reaction forces, mid-span displacement, and support rotations occurred in test beams under sequential impact loading is discussed in this section. The test results of the impact loading test are summarized in Table 10. According to previous research [35,36], the test beam can be considered to fail when the reaction force is abruptly decreased. Hence, the failure criteria were adopted based on the variation of the maximum reaction force in this study. Based on the static test, the NC-NN and NR-NN were set as the control specimens. Due to the great strengthening behavior exhibited in the static loading test, NC-3J, NC-4J, and NC-2J were adopted and evaluated for their impact resistance properties.

Table 10. Results of the impact test for the beams.

	Blow No.	Impact Properties		$D_{max.}$ (mm)	D_{res} (mm)	θ_{max} (^{0})	F_r (kN)	Remarks
		H (mm)	E_i (kJ)					
NC-NN	1			83.1	-	4.3	157.7	shear failure
NC-3J	1			66.8	53.6	3.5	152.3	spalling
	1			39.0	25.2	2.0	188.3	
NC-4J	2	2000	5.9	55.6	34.2	4.2	169.8	flexural failure
	3			-	-	-	105.2	
NR-NN	1			40.9	36.6	2.1	185.9	spalling

E_i = Impact energy; D_{max} = Max. midspan displacement; D_{res} = Residual midspan displacement; θ_{max} = Calculated support rotation; and F_r = Max. reaction force.

The top surface of NSC beams without the HSDC strengthening (NC-NN, NR-NN, and NC-3J) exhibited shear failure and spalling damage modes, respectively, in the first impact. This again proved that the fiber-reinforced concrete can effectively resist spalling damage (an approximately circular shape sunken on the impact face of the concrete specimen accompanied with the ejection of the test specimen concrete fragments) under impact load testing. Instead, the impact blow increased as the number of HSDC strengthening sides increased, moreover, enhancing the shear resistance in terms of the impact force. Even though the NC-3J exhibited spalling failure mode, this effectively reduced the ejection of fragments. The NC-4J also exhibited a flexural failure mode under impact loading.

All test beams were without any bond failure between NSC to HSDC, and only NC-4J incurred moderate damage after the first impact blow. The beam with less than 2^0 of support rotation in the impact loading test were defined to have moderate damage as recommended by UFC-3-340-02 [37]. Figure 13 shows the mid-span displacement and support reaction forces of the test beams. All the test beams were around the ultimate state range, with over 150 kN of reaction forces. In the mid-span displacement related to the time curves, this shows that the increasing number of HSDC strengthening sides decreases the maximum displacement. In general, the increasing number of HSDC strengthening sides can effectively increase the ductility and stiffness of RC beams against impact loads.
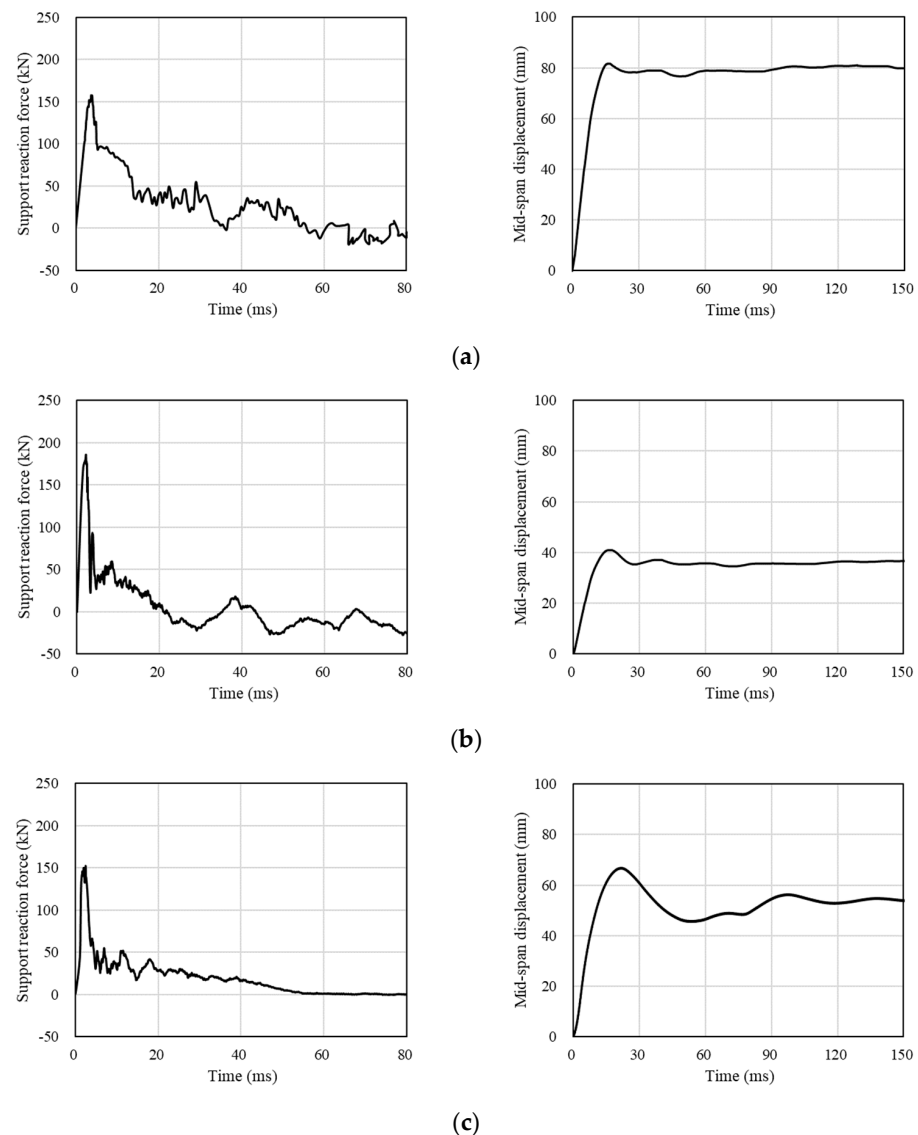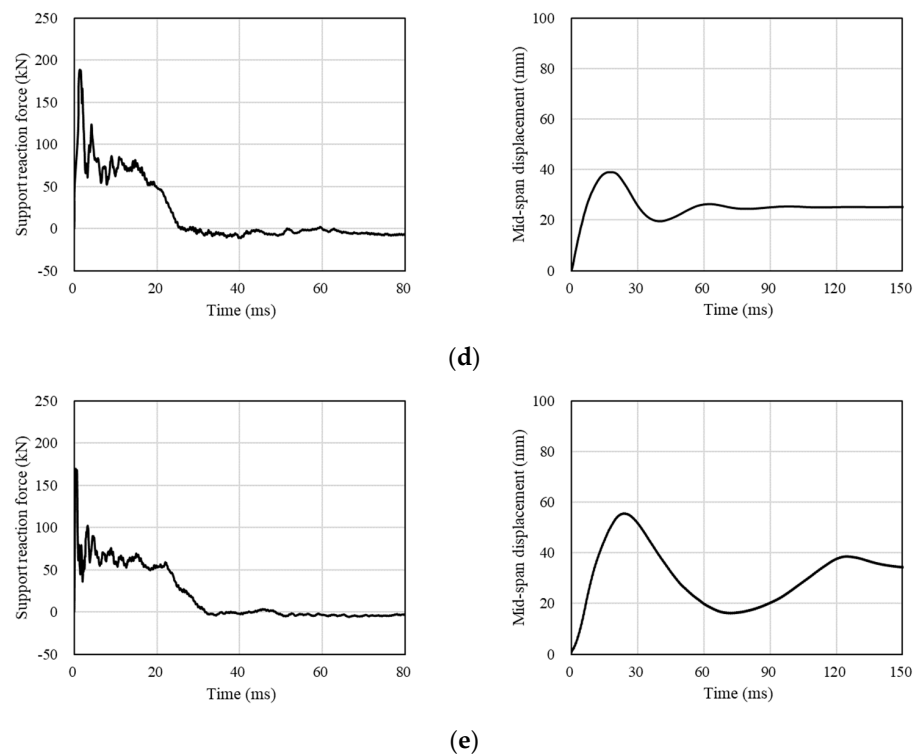

(a)

(b)

(c)

Figure 13. *Cont.*

(d)

(e)

Figure 13. Mid-span displacements and support reaction forces for test beams. (**a**) NC−NN (first blow). (**b**) NR−NN (first blow). (**c**) NC−3J (first blow). (**d**) NC−4J (first blow). (**e**) NC−4J (second blow).

4.4. Performance of Test Wall with Different Strengthening Method

4.4.1. Shielding Effectiveness of Specimens before Damage

The EMI shielding effectiveness of specimens with different materials are displayed in Figure 14a. The specimen strengthened with metallic mesh demonstrated an increase in the shielding effectiveness with a decrease in mesh size, which were approximately 1.2–17.7-, 3.8–14.9-, and 5.3–20.0-times higher, respectively, compared with specimens without a metallic mesh. This is because the metallic mesh deadens the penetration due to the continuous electrical pathway, and the metallic mesh creates a reflection interface that deadens the transmission wave in the concrete matrix [38,39].

(a)

(b)
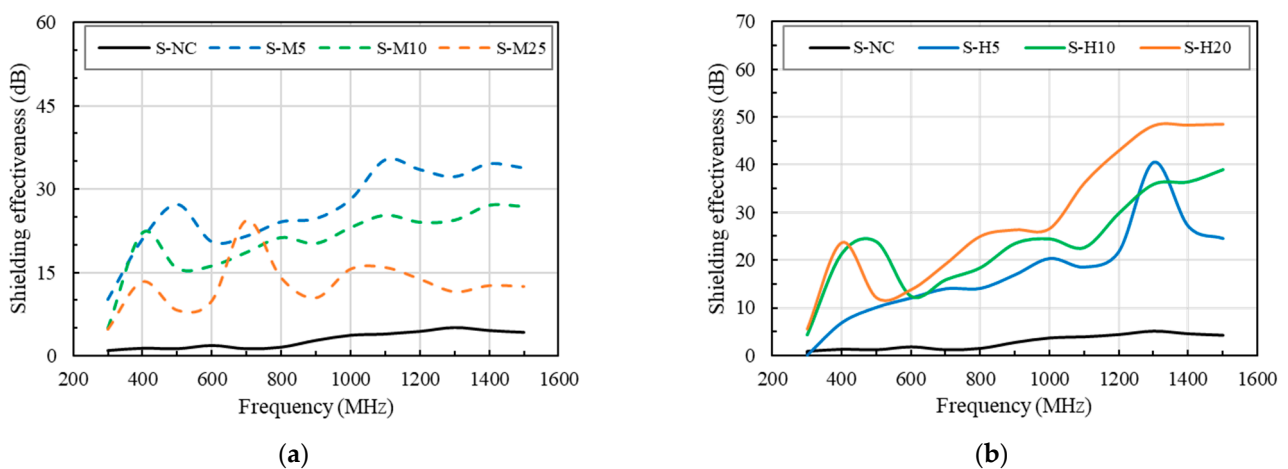
Figure 14. The shielding effectiveness of specimens. (**a**) Specimens strengthened by metallic mesh. (**b**) Specimens strengthened by HSDC.

The shielding effectiveness of a wall strengthened with metallic mesh was significantly influenced by spacing of metallic mesh layers. The specimens strengthened with different sizes and layers of metallic meshes created crests and troughs with different frequencies, which was due to the resonances at those frequencies [31,40].

This can be simply calculated through the equation $f_{mnl} = 1/(2d\sqrt{\mu\varepsilon}$ (μ = magnetic permeability of concrete, and ε = permittivity of free space) [41]. Thus, the shielding effectiveness of specimens shows waved behavior in Figure 14a. The results of the EMI shielding effectiveness test for specimens strengthened by HSDC with different thicknesses are displayed in Figure 14b. The shielding effectiveness not only increased at the same test frequency but also increased as the frequency was increased according to the HSDC thickness increase in the test specimens.

Based on the previous research [41,42], when the space of two strengthened layers had approximately 1/4 of the propagating wavelength multiplied by an odd number, this caused the cancellation of reflected waves of the first and second HSDC layers at the matrix of the absorber materials. These phenomena are displayed in Figure 14b, and negative resonance peaks move to the lower frequencies with increasing HSDC thickness. Furthermore, the specimens strengthened with HSDC mainly affected the high frequency shielding effectiveness compare with specimens strengthened with metallic mesh in the same-thickness walls.

4.4.2. Drop-Weight Impact Resistance Capacity of Walls

The drop-weight impact load test results of small-sized walls with different strengthening methods are displayed in Table 11, which include the blow number, maximum reaction force (F_r), maximum deflection (D_{max}), and crack number versus crack width (W_{max}).

The test walls strengthened with HSDC and mesh exhibited a greater Fr and many impact blows compared with the specimen S-NC. As a result, these test walls were able to undergo greater F_r before failure, which was approximately 5.7–12.2- and 4.1–6.4-times higher than those of S-NC. The F_r and crack numbers exhibited that damage intensity has a proportional relationship with the depth of HSDC strengthening of test walls. However, for test walls strengthened by different metallic mesh sizes, this was reversed. It was interesting to observe that test wall S-H5 showed a similar F_r compared with test wall S-M5. The test walls strengthened with 10 mm or more of HSDC external strengthening exhibited approximately 1.2–1.9-times the F_r seen from S-M5.

For the metallic-mesh-strengthened test walls, decreasing the mesh size could have a limited influence on the development of mid-point displacement before failure and concrete debris, which is similar to previous research [31,36,43]. The increase in the HSDC strengthening thickness decreased the D_{max} particularly for the impact test performed on S-H20. The test walls under the first impact load exhibited both radial and radioactive cracking on the bottom surface with crack widths ranging from 0.05 to 0.15 mm, and less visible cracks and limited scabbing occurred after the first impact blow.

Succeeding impact blows led to diagonal fractures in the test wall, and large diagonal cracks were obvious on the bottom side of test wall. Despite this, the test walls maintained their integrity, and the cracks were prevented from opening as a result of mesh crossing and fiber bridging (HSDC). Otherwise, reductions in strengthening the metallic mesh size reduced W_{max} and the development, D_{max}, as well as the magnitude of damage at the bottom side of test wall. Compared with the metallic mesh strengthening, the strengthened with HSDC was effective in controlling those properties. Similar characteristics can be verified through evaluating the energy dissipation (Table 11); thus, 5 mm of metallic mesh and 20 mm of HSDC were selected to evaluate the large-sized wall strengthening properties under impact loading.

Table 11. Results of the impact tests for small-sized walls.

	Blow No.	Impact Properties		F_r (kN)	$D_{max.}$ (mm)	Crack Numbers	W_{max} (mm)	E_{dis} (kJ)
		H (mm)	E_i (kJ)					
S-NC	#1	200	0.20	16.2	-	-	-	-
S-M5	#1	200	0.20	19.8	0.90	6	0.05	
	#2	300	0.49	23.1	1.03	6	0.08	
	#3	400	0.88	30.7	1.74	11	0.15	1.89
	#4	500	1.37	29.9	1.75	15	0.75	
	#5	600	1.96	25.0	3.82	15	3.08	
S-M10	#1	200	0.20	22.6	0.74	4	0.05	
	#2	300	0.49	24.6	0.98	8	0.15	
	#3	400	0.88	26.4	1.34	8	0.90	1.31
	#4	500	1.37	26.4	1.34	11	1.20	
	#5	600	1.96	24.0	3.77	12	1.70	
S-M25	#1	200	0.20	20.6	1.33	4	0.08	
	#2	300	0.49	21.8	1.00	6	0.45	
	#3	400	0.88	27.2	1.89	9	0.80	0.83
	#4	500	1.37	24.5	2.06	10	1.40	
S-H5	#1	200	0.20	19.7	1.05	4	0.45	
	#2	300	0.49	22.8	1.54	6	1.10	
	#3	400	0.88	23.7	2.22	9	1.95	1.28
	#4	500	1.37	26.2	2.48	9	5.00	
	#5	600	1.96	15.0	4.63	9	6.00	
S-H10	#1	200	0.20	22.2	0.73	5	0.25	
	#2	300	0.49	24.4	1.07	11	1.30	
	#3	400	0.88	24.4	1.91	14	2.00	
	#4	500	1.37	25.8	1.64	16	4.50	1.87
	#5	600	1.96	28.1	1.75	26	5.50	
	#6	700	2.65	20.0	3.69	26	3.00	
S-H20D	#1	200	0.20	23.6	0.49	5	0.05	
	#2	300	0.49	28.9	0.72	8	0.20	
	#3	400	0.88	32.1	0.97	13	0.40	
	#4	500	1.37	26.4	1.13	21	0.70	2.54
	#5	600	1.96	38.7	1.47	29	1.10	
	#6	700	2.65	38.5	1.77	29	2.00	
	#7	800	3.43	21.0	3.04	29	4.00	
L-M5	#1	2000	5.88	923.6	17.85	24	2.15	
	#2	2000	11.76	529.9	27.60	26	scabbing	3.52
L-H20	#1	2000	5.88	1025.2	18.72	35	1.45	
	#2	2000	11.76	823.9	27.61	67	2.15	3.70
	#3	2000	17.56	559.1	20.14	67	scabbing	

H = Drop height; E_i = Impact energy; F_r = Max. reaction force; $D_{max.}$ = Max. midspan displacement; W_{max} = Max. crack width; and E_{dis} = Energy dissipation.

The impact loading test results of large walls exhibited similar behavior compared with small-sized walls. The test wall L-H20 exhibited great impact resistance properties compared with L-M5 at the first and second blow, which is a result of the hybrid fiber increasing crack number, energy distribution capacity, and reduced crack width. Test walls L-M5 and L-H20 observed scabbing damage in the second and third blows, respectively; however, the fragmentation largely decreased in L-H20. Although they exhibited serious scabbing damage, they maintained their residual structural performance and EMI shielding effectiveness after damage, thus, further demonstrating the EMI shielding effectiveness. The observed damage after the final impact of the test walls is shown in Figure 15.
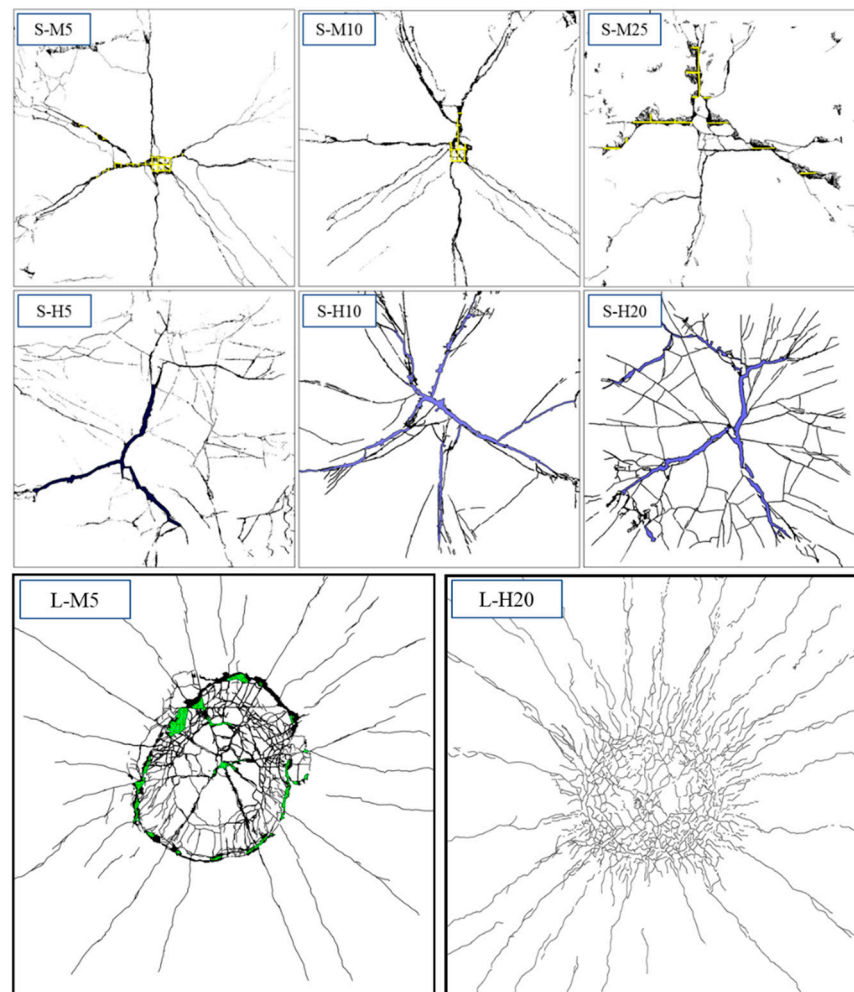
Figure 15. Observed damage after the final impacts of the test walls.

4.4.3. Shielding Effectiveness of Specimens after Damage

The S-H5 specimen saw the largest shielding decrease ratio compared with all test walls, which was approximately 28.1% (Figure 16). This is because large crack widths were exhibited on the bottom side radial of the impact region for S-H5, which significantly decreased the effective thickness of the wall. This supported the view [31] that the shielding effectiveness of concrete walls is mainly influenced by the effective thickness variation, which is affected by external loads or environment factors. Concrete walls strengthened with 20 mm of HSDC (L-H20) recorded the smallest shielding-effectiveness-decrease ratio with a value of approximately 15.2% after the impact damage area ratio (6.7%). For the test walls strengthened by metallic mesh, the shielding-effectiveness-decrease ratio was reduced accordantly with the reduced metallic mesh size.

A smaller metallic mesh mainly influenced the number of cracks developed and decreased the scabbing of the bottom side of the concrete wall. Therefore, S-M5 recorded the smallest shielding-effectiveness-decrease ratio with a value of approximately 1.7% after the impact damage area ratio (4.31%). Compared with the metallic mesh strengthening, concrete walls strengthened with HSDC decreased the shielding-effectiveness-decrease ratio. This is due to the uniformly distributed fiber, although multiple cracks were exhibited, which decreased the effective thickness of concrete wall, the shielding-effectiveness-decrease ratio indicated similar values in similar impact damage area ratios of walls without different strengthening thickness.
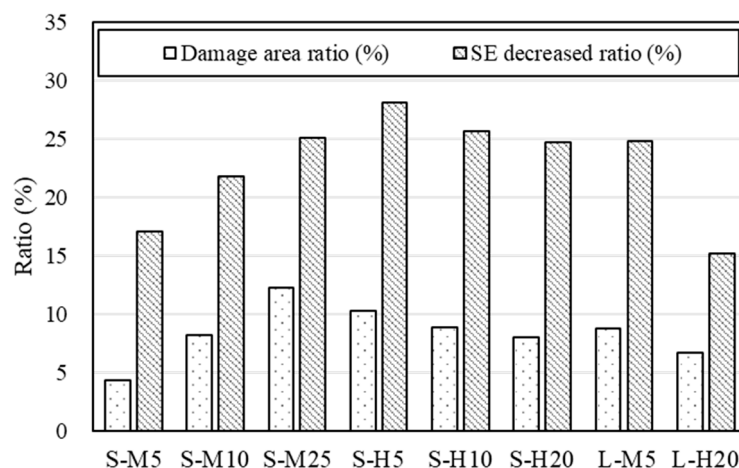
Figure 16. The shielding-effectiveness-decrease ratio after damage.

5. Concluding Remarks

This study utilizes a building information modeling-based approach to simulate strategic locations of Shelter in Place and a strengthening method, which includes impact and electromagnetic interference shielding effectiveness. From this investigation, the following conclusions can be drawn:

(1). Subway stations are Designated Facilities for Public Use facilities in a CBRE situation, and spaces for SIP must be designated inside the stations. However, if you look at the provided Station Evacuation Route Map (Figure 1), most of the stations' evacuation routes are from the platform to the tunnel or to the outside, and, in most places, a separate evacuation space is not specified. The domestic evacuation time standards limit the evacuation time from outside to the SIP facility in a CBRE situation [43] and suggest evacuating to a safe space or outside within 6 min in the case of an emergency situation in the subway [4]. Therefore, in this study, the method that was the most efficient between moving outside in the case of an emergency situation or moving to SIP when an evacuation space for SIP is designated was studied.

As a result, the time taken to evacuate to the outside exit (Scenario A) was 529.6 s, which was 293.5 s longer than the 236.1 s (Scenario D) of moving to the SIP. This is because, when moving outside, a large number of people evacuated through a narrow exit, creating bottlenecks, such as stairs and subway gates. Therefore, through this study, we found that moving inside to a determined SIP was much more efficient than moving outside in the case of an emergency inside the subway as well as in CBRE situations. However, since the location of the SIP in the Evacuation Map provided to existing subway stations is not specified, an appropriate location of the SIP is suggested in this study, and appropriate ventilation and blocking facilities are needed.

(2). Although the subway station evacuation time is affected by shape information, such as stairs and doors [5,6], Yangjae Station, which was used in this study, is a transfer station where Line 3 and Shinbundang Line meet, and evacuation takes place in a wide space. Therefore, the most time loss occurs as a bottleneck when passing through a gate rather than a door or stairs. In the case of the gate, it is possible to move in only one direction; additionally, there is a waiting time for approval after touching the transportation card when moving. In other words, when evacuees move in the case of an emergency situation, they could be allowed to pass in both directions and move without a traffic card. Of course, in the case of Scenario E, which does not require many gates, the evacuation time was hardly affected; however, we analyzed that it was affected by a minimum of 8.8 s and a maximum of 271.7 s. This is the easiest way to shorten the evacuation time in the case of an emergency, and it is necessary to

review the improvement of the gate through this study as it is a situation that could cause casualties over time.

(3). For test beams, increasing the number of HSDC strengthening sides decreases the maximum displacement, effectively increasing the ductility and stiffness of RC beams against impact loads. The walls strengthened with metallic mesh recorded an increase in shielding effectiveness with a decrease in mesh size and increased HSDC thickness strengthening. Furthermore, a similar phenomenon occurred for impact load testing, and the shielding effectiveness ratio decreased after damage. Thus, concrete elements of shelter in place strengthened by 5 mm metallic mesh and/or HSDC can be chosen due to the application aim of static, impact, and shielding effectiveness.

References

1. American Red Cross. *Fact Sheet on Shelter-In-Place*; American Red Cross: Washington, DC, USA, 2003.
2. Anti-Corruption & Civil Rights Commission. Improving the Effectiveness of Evacuation Facility Guidance to Ensure the Safety of Residents. January 2015. Available online: https://www.acrc.go.kr/board.es?mid=a10504030000&bid=1013&act=view&list_no=30352 (accessed on 5 January 2015).
3. Ministry of Land, Infrastructure and Transport. Notice No. 2018-199, 2018.3.28. Full revision, Design Guidelines for Convenience Facilities at Transit Stations for Urban Railroad Stations. Available online: https://www.law.go.kr/LSW/admRulInfoP.do?admRulSeq=2100000118529 (accessed on 28 March 2018).
4. Kim, Y.-H.; Choi, J.-S.; Yuan, T.-F.; Yoon, Y.-S. Building-Information-Modeling Based Approach to Simulate Strategic Location of Shelter in Place and Its Strengthening Method. *Materials* **2021**, *14*, 3456. [CrossRef] [PubMed]
5. Kim, Y.-H.; Yoo, S.-J.; Yuan, T.-F.; Yoon, Y.-S. Effect of design code and evacuation information on strategic location of Shelter in Place (SIP) in light rail station. *J. Asian Arch. Build. Eng.* **2021**, *21*, 1332–1347. [CrossRef]
6. Zou, Q.; Chen, S. Simulation of Crowd Evacuation under Toxic Gas Incident Considering Emotion Contagion and Information Transmission. *J. Comput. Civ. Eng.* **2020**, *34*, 04020007. [CrossRef]
7. Gupta, A.; Yadav, P. SAFE-R: A new model to study the evacuation profile of a building. *Fire Saf. J.* **2004**, *39*, 539–556. [CrossRef]
8. Society of Fire Protection Engineers. *SFPE Handbook of Fire Protection Engineering*, 3rd ed.; National Fire Protection Association: Quincy, MA, USA; Society of Fire Protection Engineers: Bethesda, MD, USA, 2002.
9. Richard, W.B.; Addison, W.A. Normal walking speed: A descriptive meta-analysis. *Physiotherapy* **2011**, *97*, 182–189.
10. Ando, K.; Ota, H.; Oki, T. Forecasting the flow of people. *Railw. Res. Rev.* **1988**, *45*, 8–14.
11. Statics Korea. Population Census Results in 2020, Release 29 July 2021. Available online: http://kostat.go.kr/portal/korea/kor_nw/1/1/index.board?bmode=read&aSeq=391020 (accessed on 29 July 2021).
12. Seoul Metro, December 2021 Number of People Using Each Station by Time Zone (Lines 1 to 8), Release 17 January 2022. Available online: http://www.seoulmetro.co.kr/kr/board.do?menuIdx=548&bbsIdx=2213467 (accessed on 17 January 2022).
13. Namuwiki Shinbundangsun 14 Statistic of Boarding and Alighting by Station. Available online: https://namu.wiki/w/%EC%8B%A0%EB%B6%84%EB%8B%B9%EC%84%A0 (accessed on 13 October 2022).
14. FEMA453. *Risk Management Series, Design Guidance for Shelters and Safe Rooms*; FEMA: Washington, DC, USA, 2006.
15. IMO. *IMO Guidelines for Evacuation Analysis for New and Existing Passenger Ships*; International Maritime Organization: London, UK, 2016.
16. Thunderhead Engineering. *Verification and Validation*; Thunderhead Engineering: New York, NY, USA, 2015; pp. 85–110.

17. Wikipedia. Seoul Subway Line 3, Rolling Stock. Available online: https://en.wikipedia.org/wiki/Seoul_Subway_Line_3 (accessed on 21 October 2022).
18. Roh, J.S.; Ryou, H.S.; Yoon, S.W. The effect of PSD on life safety in subway station fire. *J. Mech. Sci. Technol.* **2010**, *24*, 937–942. [CrossRef]
19. Korea National Railway. Convenience Facility Design for the Handicapped. Available online: https://www.kr.or.kr/boardCnts/fileDown.do?fileSeq=7cb186ca4d90c62df06f67aa4177beb6 (accessed on 27 June 2019).
20. Templer, J.A. *The Staircase: Studies of Hazards, Falls and Safer Design*; MIT Press: Cambridge, MA, USA, 1992.
21. Main Design Criteria for Subway (Facility Field), in the Design Standard for Subway. 2018. Available online: http://news.seoul.go.kr/citybuild/archives/200564 (accessed on 29 June 2022).
22. Yuan, T.-F.; Lee, J.-Y.; Min, K.-H.; Yoon, Y.-S. Experimental Investigation on Mechanical Properties of Hybrid Steel and Polyethylene Fiber-Reinforced No-Slump High-Strength Concrete. *Int. J. Polym. Sci.* **2019**, *2019*, 4737384. [CrossRef]
23. Yuan, T.-F.; Lee, J.-Y.; Yoon, Y.-S. Enhancing the tensile capacity of no-slump high-strength high-ductility concrete. *Cem. Concr. Compos.* **2020**, *106*, 103458. [CrossRef]
24. Yuan, T.-F.; Hong, S.-H.; Shin, H.-O.; Yoon, Y.-S. Bond Strength and Flexural Capacity of Normal Concrete Beams Strengthened with No-Slump High-Strength, High-Ductility Concrete. *Materials* **2020**, *13*, 4218. [CrossRef]
25. *ASTM C150*; Standard Specifcation for Portland Cement. ASTM International: West Conshohocken, PA, USA, 2007.
26. Lee, J.Y.; Kim, D.B.; Kwon, K.Y.; Yoon, Y.S. Recommendation of Adequate Sampling Rate for Drop Weight Impact Test with Application of Nyquist's Sampling Theorem. *J. Korean Soc. Hazard Mitig.* **2015**, *15*, 61–67. [CrossRef]
27. Lee, J.-Y.; Yuan, T.; Shin, H.-O.; Yoon, Y.-S. Strategic use of steel fibers and stirrups on enhancing impact resistance of ultra-high-performance fiber-reinforced concrete beams. *Cem. Concr. Compos.* **2020**, *107*, 103499. [CrossRef]
28. Micheli, D.; Marchetti, M.; Pastore, R.; Vricella, A.; Gradoni, G.; Moglie, F.; Primiani, V.M. Shielding effectiveness of carbon nanotube reinforced concrete composites by reverberation chamber measurements. In Proceedings of the 2015 International Conference on Electromagnetics in Advanced Applications (ICEAA), Turin, Italy, 7–11 September 2015; pp. 145–148. [CrossRef]
29. Micheli, D.; Pastore, R.; Vricelaa, A.; Delfni, A.; Marchetti, M.; Santoni, F. *Electromagnetic Characterization of Masterials by Vector Network Analyzer Experimental Setup, Spectroscopic Methods for Nanomaterials Characterization (Micro and Nano Technologies)*; Elsevier: Amsterdam, The Netherlands, 2017; pp. 195–236.
30. Yuan, T.-F.; Choi, J.-S.; Hong, S.-H.; Yoon, Y.-S. Enhancing the electromagnetic shielding and impact resistance of a reinforced concrete wall for protective structures. *Cem. Concr. Compos.* **2021**, *122*, 104148. [CrossRef]
31. Lampropoulos, A.P.; Paschalis, S.A.; Tsioulou, O.T.; Dritsos, S.E. Strengthening of reinforced concrete beams using ultra high performance fibre reinforced concrete (UHPFRC). *Eng. Struct.* **2016**, *106*, 370–384. [CrossRef]
32. Tanarslan, H. Flexural strengthening of RC beams with prefabricated ultra high performance fibre reinforced concrete laminates. *Eng. Struct.* **2017**, *151*, 337–348. [CrossRef]
33. Al-Osta, M.; Isa, M.; Baluch, M.; Rahman, M. Flexural behavior of reinforced concrete beams strengthened with ultra-high performance fiber reinforced concrete. *Constr. Build. Mater.* **2017**, *134*, 279–296. [CrossRef]
34. Hrynyk, T.D.; Vecchio, F.J. Behavior of Steel Fiber-Reinforced Concrete Slabs under Impact Load. *ACI Struct. J.* **2014**, *111*, 1213–1223.
35. Lee, J.-Y.; Shin, H.; Yoo, D.-Y.; Yoon, Y.-S. Structural response of steel-fiber-reinforced concrete beams under various loading rates. *Eng. Struct.* **2018**, *156*, 271–283. [CrossRef]
36. Defence USDo. *Unified Facilities Criteria (UFC) 3-340-02: Structures to Resist the Effects of Accidental Explosions*; Department of Defense: Washington, DC, USA, 2008.
37. Yuan, T.-F.; Choi, J.-S.; Kim, S.-K.; Yoon, Y.-S. Assessment of Steel Slag and Steel Fiber to Control Electromagnetic Shielding in High-Strength Concrete. *KSCE J. Civ. Eng.* **2021**, *25*, 920–930. [CrossRef]
38. Hyun, S.Y.; Kyoung, J.K.; Lee, H.J.; Lee, K.W.; Yook, J.G. Analysis of shielding effectiveness of reinforced concrete against high altitude electromagnetic pulse. *IEEE Trans. Electromagn. Compat.* **2014**, *56*, 1488–1496. [CrossRef]
39. Liu, F.; Lü, X.; Li, Y.B.; Yang, J.; Pan, Z. Attenuation characteristics on high power microwave penetrating through reinforcement nets. *High Power Laser Part. Beams* **2012**, *24*, 2713–2717. [CrossRef]
40. Lu, H.D.; Zhu, F.; Li, X.; Tang, Y.T. Shielding effectiveness of reinforced concrete toward electric arcs in pantograph catenary systems of metro. *Chin. J. Radio Sci.* **2016**, *31*, 1209–1215. [CrossRef]
41. Shukla, V. Review of electromagnetic interference shielding materials fabricated by iron ingredients. *Nanoscale Adv.* **2019**, *1*, 1640–1671. [CrossRef] [PubMed]
42. Sadraie, H.; Khaloo, A.; Soltani, H. Dynamic performance of concrete slabs reinforced with steel and GFRP bars under impact loading. *Eng. Struct.* **2019**, *191*, 62–81. [CrossRef]
43. National Fire Agency 2009 Policy Research Report. In *Study on CBR Evacuation Facility Standards and Utilization Plans*; Hanseo University: Seosan, Republic of Korea, 2009; p. 49.